Title: Assessment of Per-Axis Thruster Control Authority of Cassini Spacecraft for Low-Altitude Titan Flybys

Siamak (Sam) Sarani[1]
Jet Propulsion Laboratory, California Institute of Technology, Pasadena, California 91109-8099

Abstract

Upon arrival at Saturn, Cassini will execute numerous low-altitude flybys of Titan and a few targeted icy satellite flybys. At the closest approach altitudes, the spacecraft must use its thrusters in order to overcome the external torques, maintain attitude control, and perform the required science slews. Because of the uncertainties associated with Titan atmospheric density model, as well as other uncertainties, the adequacy of thruster control authority at the closest approach must carefully be assessed to ensure that Cassini will not tumble out of control. The results indicate that even with conservative assumptions, there still exists adequate control authority margin.

Introduction

1. Cassini Spacecraft

Cassini was launched on October 15, 1997 from Cape Canaveral Air Force Station using a U.S. Air Force Titan IV-B/Centaur launch vehicle. The launch vehicle was made up of a two-stage Titan IV booster rocket, two strap-on solid rocket motors, the Centaur upper stage, and a payload enclosure or fairing. The complete Cassini flight system was composed of the launch vehicle and the spacecraft. The spacecraft is a combined Saturn orbiter (built by NASA) and Titan atmospheric probe, named the Huygens probe, manufactured by the European Space Agency (ESA). The Huygens probe is a large probe equipped with a parachute and is designed to be separated from Cassini obiter, possibly on the third flyby of Titan, and land on Titan.

The Cassini spacecraft, including the orbiter and the Huygens probe, is one of the largest, heaviest, and most complex interplanetary spacecraft ever built. The complexity of the spacecraft is necessitated both by its trajectory or flight path to Saturn and by the ambitious program of scientific observations to be undertaken once the spacecraft reaches its destination (in July 2004). The orbiter alone weighs 2,150 kg (4,750 pounds). When the 350-kilogram Huygens probe, launch vehicle adapter, and 3,132 kg (6,905 pounds) of propellants were loaded, the spacecraft weighed about 5,600 kilograms (12,346 pounds) at launch. Only the two Phobos spacecraft sent to Mars by the former Soviet Union were heavier. The Cassini spacecraft stood more than 6.8 meters (22.3 feet) high and was more than 4 meters (13.1 feet) wide. It will function with 1,630 interconnect circuits, 22,000 wire connections, and over 14 kilometers (8.7 miles) of cabling. It is a three-axis stabilized spacecraft equipped for 27 diverse science and investigations with 12 orbiter and 6 Huygens probe instruments, one high gain and two low gain antennas, three Radioisotope Thermal Generators (RTGs) for power, main engines, attitude thrusters, and reaction wheels. The Cassini spacecraft with its magnetometer boom deployed is shown in Figure 1.

2. Cassini Mission

The Cassini-Huygens mission, managed by Jet Propulsion Laboratory, is an international venture involving the NASA, ESA, and several separate academic and industrial partners. The mission will explore the Saturnian system. In order to reach the ringed planet with such a rich complement of science instruments, Cassini has gathered energy from launch and flybys of planets in the inner solar system during its interplanetary cruise of almost seven years. Beginning July 2004, upon arrival at Saturn, a large injection

[1] AACS Technical Staff, Mail Stop 230-104D, Avionic Systems Engineering Section, 4800 Oak Grove Drive.

burn is executed to insert the spacecraft in Saturn orbit, and a four-year primary science tour (and a possible extended tour) of the system is begun.

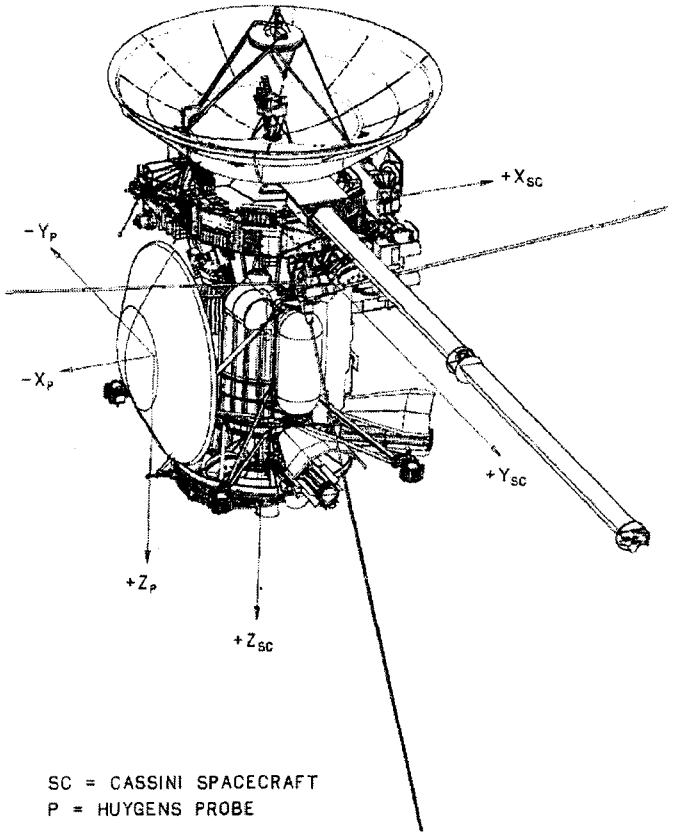

Figure 1 - Cassini spacecraft with deployed magnetometer boom and attached Huygens probe

The mission is designed to conduct scientific investigations of the planet Saturn and its rings, magnetosphere, icy satellites, and Saturn's largest moon, Titan. Each flyby will emphasize different science objectives such as Remote Sensing, Radar Mapping, and Radio Sciences. The targeted icy satellite flyby altitudes will be less than or equal to approximately 1000 km and will consist of three flybys of Enceladus and a single flyby of each of Iapetus, Rhea, Hyperion, and Dione.

Upon arrival at Saturn, Cassini will execute numerous low-altitude flybys of Titan. The tour of Titan will include some 44 targeted flybys of which 24 are close encounters at altitudes ranging from 949 to 956 km. A *targeted* flyby is one where the orbiter's trajectory has been designed to pass through a specified aim point (latitude, longitude, and altitude) at closest approach. At Titan, the aim point is selected to produce a desired change in the trajectory using the satellite's gravitational influence. If the closest approach point during a flyby is far from the satellite, or if the satellite is small, the gravitational effect of the flyby can be small enough that the aim point at the flyby need not be tightly controlled. Such flybys are called *non-targeted.* Flybys of Titan at distances greater than 25,000 km are considered non-targeted flybys. The first flyby altitude relative to Titan is about 1200 km with a flyby velocity of approximately 6 km/s.

3. Titan Atmospheric Model

Because of atmospheric effects on Cassini, there exists a need to analyze Titan's atmosphere in order to determine the range of safe flyby altitudes (for RWA and for RCS control). In fact, at low altitudes (1200 km or less), the torque due to the atmospheric drag is so high that the reaction wheels are unable to absorb the momentum and the thruster attitude control of the spacecraft is required.

Titan is the only known moon with a thick atmosphere. Like Earth, Titan's atmosphere is mainly nitrogen. By analogy with Earth, Titan's atmosphere is subdivided into regions defined by the temperature variations with altitude or pressure, the two being connected through the hydrostatic law. These regions and their associated altitude range are: *troposphere* (0 – 50 km), *stratosphere* (50 – 300 km), *mesosphere* (300 – 600 km), *thermosphere* (600 – 1200 km), and finally *exosphere* (1200 – 3500 km). More than half of the targeted flybys of Titan are in thermosphere region in which the temperature rises from ~140 K (at 600 km) to ~ 190 K (at 1200 km).

In late 1980, Voyager 1 visited Saturn system and gave us our first look at Titan, the Saturn's largest satellite, and its atmosphere. Its trajectory carried Voyager 1 past Titan with the closest approach at a distance of roughly 6500 km. The UVS on-board Voyager 1 made a number of observations at Titan, including disk-averaged spectra of Titan's day-glow, measurements of emission as a function of altitude (limb drift), and solar occultations by atmosphere.

A number of Titan atmosphere models of increasing complexity have been investigated all of which are based on Voyager I flyby information. The first Titan atmosphere model was suggested by Lellouch and Hunten in a report published in 1987. This model was then superseded by so-called Yelle's engineering model in 1992 after publishing a report by Yelle, Strobell, Lellouch, and Gautier [14].

Strobel supplied another atmospheric model in March 93, which included number density (in cm^{-3}), temperature (in K), and mass density (in gm/cm^3) as functions of the altitude (in km) with 50% confidence. The maximum (3σ) model used with this recommended model is identical to the maximum model developed by Yelle. The Strobel recommended model has consistently lower densities than the Lellouch/Hunten recommended model. However, the Strobel maximum model has higher densities than the Lellouch/Hunten maximum model at altitudes above 900 km.

Yelle provided JPL with a model of Titan atmosphere that included pressure (in $dyne/cm^2$), density (in gm/cm^3), temperature (in K), and atomic mass (in amu) as functions of altitude (in km). Yelle's Titan atmosphere model was endorsed by Cassini Program Office in October 1993 and has been used since then as the official Titan atmospheric model [8]. According to Yelle Titan atmospheric model, Titan atmosphere consists of 95% nitrogen, 3% methane, and 2% argon. Three sets of data were provided, one set with a 50% confidence (the so-called "recommended" model associated with 0σ), and the others with 99.87% confidence (minimum and maximum models associated with $\pm 3\sigma$). Each model covers altitudes from zero to 3000 km and provides number densities for Nitrogen, Methane, and Argon, total number density, and mass density along with pressure and temperature. The three models span the modeling uncertainty of the atmosphere. The recommended model is the adopted best estimate. Most of the variation between the models in the upper atmosphere in this model is due to uncertainty in the temperature, and by varying temperature linearly with the σ value, the density can be computed assuming hydrostatic equilibrium.

Adler in a memo [9] distributed in March 1995 derived a formula using the tabulated densities versus stratosphere temperature and altitude provided by Yelle using the MATHEMATICA software tool (see equation 3). The three terms in his formula are for Nitrogen, Methane, and Argon in that order. The density, ρ, is a function of the altitude, z, and the figure 2575 km is the radius of Titan. The range of altitudes used is from 925 km to 3000 km. For this range of altitudes, the recommended temperature is 175 K. The temperature is used to span the uncertainty in this atmosphere model. If n the number of σ's to deviate from the median (recommended) model, then $T = 175 + 10n$, e.g. -3σ (minimum) model is obtained with $T = 145K$, and $+3\sigma$ (maximum) model is obtained with $T = 205$ K. The values of n outside -3σ to $+3\sigma$ should never be used. The altitude z can range from 800 km to 3000 km. Over this range, the formula matches the tabulated values for all three models to within 1% of the altitude. For altitudes between 800 and 1600 km, the formula is accurate within 10 km of the tabulated data.

Strobel et al. reexamined the Voyager Ultraviolet Spectrometer (UVS) solar occultation data of Smith et al. (1982) and discovered that their suggested model thermosphere was not consistent with their observed optical depth profiles, particularly those dominated by CH_4, which were not internally consistent. Vervack (in 1997) undertook a detailed reanalysis of the Voyager 1 solar occultation data [15]. The ingress data had a

higher quality than the egress data, and was, therefore, used to derive a modified atmospheric model. This atmospheric model is an isothermal model, with variable gravitational acceleration, and can be applied over an altitude range of 700-2000 km without substantial error, as long as it is remembered that extrapolation is involved above 1450 km and below 850 km. No argon was detected in the UVS occultation data and hence was not included in this atmospheric model. According to this model, the atmospheric density is slightly higher than that of Yelle's model for 950 km altitude, but coincides with Yelle's model at 500 km and 1300 km altitudes.

It should be mentioned again that Cassini Program Office continues to use Yelle's Titan atmosphere model at least until the first Titan flyby is completed and both the Ion Neutral Mass Spectrometer (INMS) measurement of Titan atmospheric density and thruster telemetry associated with the first Titan flyby are analyzed. The model with then be assessed for its applicability.

4. Reaction Control System

The Cassini spacecraft is 3-axis stabilized. In order to maintain a stable attitude during the course of its mission, two distinct control systems are used: the Reaction Control System (RCS), and the Reaction Wheel Assembly (RWA) control system. RCS is responsible for maintaining 3-axis attitude control just like the RWA control system. However, functionally RCS performs a very different role.

During most of the cruise phase and for selected points in its encounter phase, the spacecraft relies on RCS. This system consists of sixteen (eight primary and eight redundant) blow-down thrusters, placed in four clusters, with a thrust range of 0.5-1.0 N, consuming monopropellant (hydrazine) thrusters. The clusters are mounted via tripods to the propulsion module, at the corners of a rectangle parallel to the X-Y plane. Each cluster has a pair of thrusters, which thrust in -Z direction (X and Y axis control thrusters) and another pair, which thrust in the ±Y direction (Z axis control thrusters). Firing of these thrusters consumes hydrazine propellant, which is stored in a tank onboard the spacecraft. A diagram of thruster locations and thrust directions is captured in Figure 2.

In particular, RCS is required to perform the following tasks: maintain 3-axis attitude control, hold the spacecraft with optimal limit cycle control during the entire cruise phase, acquire the sun following separation from the launch vehicle, point the fixed telecommunications antenna (high and low gain antennae, that is HGA and LGA) toward Earth, point the HGA toward the probe for probe relay tracking, perform commanded turns of the spacecraft as required for trajectory correction maneuvers as well as for other purposes such as science observations during Titan flybys, detumble the spacecraft after Centaur separation and probe release, RWA momentum unloading, full sky spiral sun acquisition upon fault situation, and perform small trajectory correction burns.

Computation of Total Applied Torque on Cassini during the Titan Flyby

In the order of importance, the three major contributors to the torque experienced by Cassini during the Titan flybys are:

- Titan atmospheric torque
  Note: This torque is only present for Titan flybys and is severe for flybys at low altitude, i.e. 950 to 1200 km
- Target motion compensation (TMC) torque to maintain the spacecraft nadir or spotlight pointed
- Torque required for science turns
  Note: The main science observations are RADAR, Optical Remote Sensing (ORS),
- *and Radio Sciences*

The analysis of the Titan flybys considers three environmental torques acting on Cassini: Titan atmospheric drag, gravity gradient, and radiation torque (due to solar radiation on the magnetometer boom and RTG radiation).

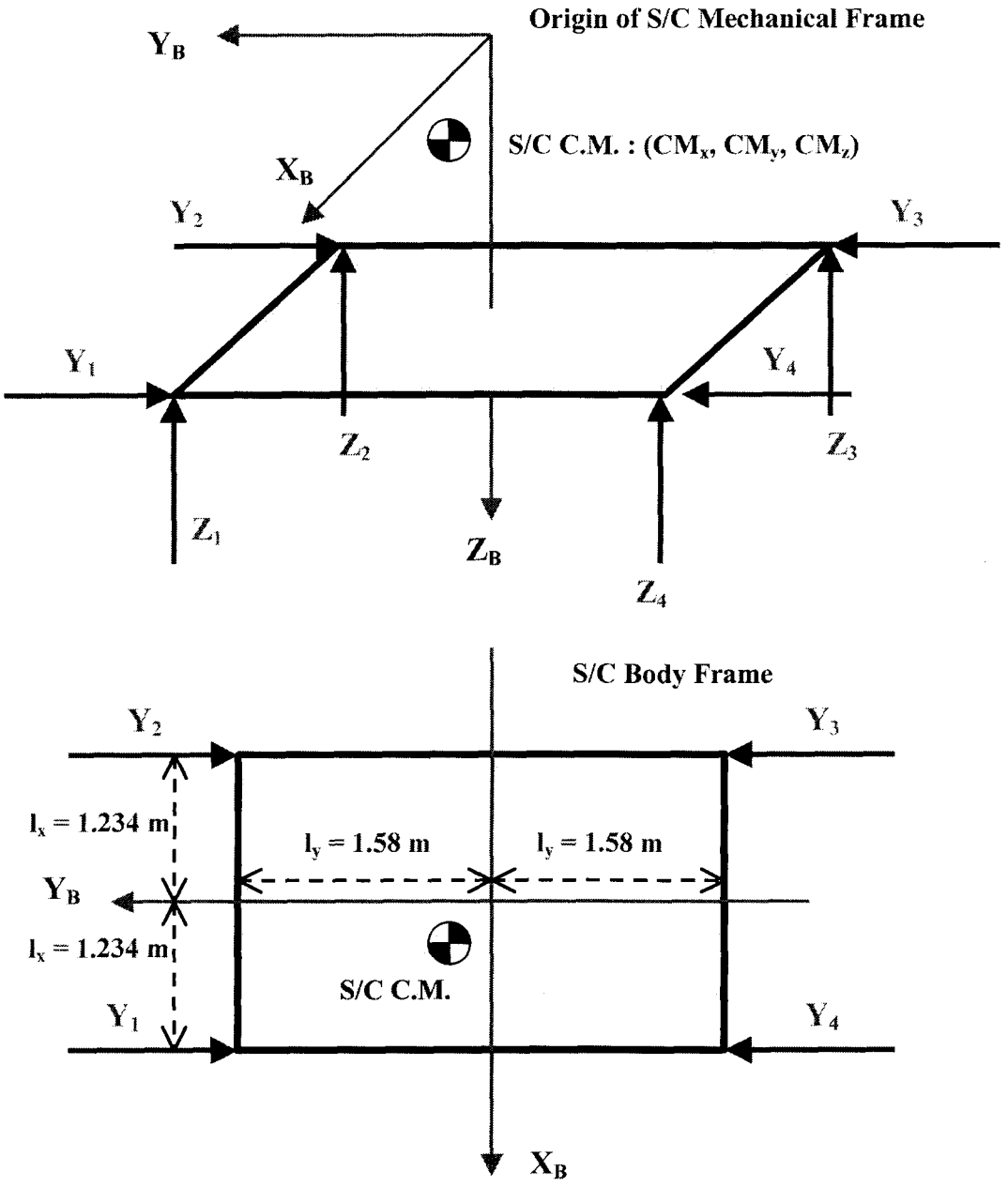

Figure 2 -Thruster locations and thrust directions

Note: The depicted center of mass is for post-probe release condition

The total torque (the sum of the drag, gravity, and radiation torques) acting on the spacecraft is determined for each of 44 targeted Titan flybys.

INMS observation attitude (-X to RAM direction, -Z to Titan) is assumed as the baseline for this analysis. The atmospheric drag pressure (applied to the worst case product of projected area and moment arm) and solar radiation pressure are assumed to act in the X-direction, causing maximum Y- and Z-axis torques (a worst-case situation). The gravity gradient torque calculations are worst-case (independent of spacecraft attitude), and the RTG torque is constant in the spacecraft body frame. When combining torques, all

torques are summed by absolute value to give worst-case analysis. Only Y- and Z-axis torques are covered here, since they are worst-case, and x-axis torque is negligible at this attitude.

From the available data it appears that Titan does not have its own magnetic field but rather interacts with and amplifies the magnetic field in its vicinity. The magnetic field at Titan can come from Saturn or the solar wind. Time-average of the field would be zero but at any time it might be of the order of 10 nT. Torque applied to spacecraft due to such a weak filed is negligible

Also, since the distance from Saturn is great, and Titan has negligible planetary and reflected solar radiation, torques due to these effects are ignored. Finally, any impacts with particles or solar wind effects are ignored.

Atmospheric Drag Torque

The equations for drag torque are:

$$\left|T_{atm-y}\right| = \left|(c.p.-c.m.)_z\right| \times \frac{1}{2} C_D \rho_{Yelle} V^2 A \qquad \text{Nm} \qquad (1)$$

$$\left|T_{atm-z}\right| = \left|(c.p.-c.m.)_y\right| \times \frac{1}{2} C_D \rho_{Yelle} V^2 A \qquad \text{Nm} \qquad (2)$$

$(c.p.-c.m.)_y$	= 0.849 m [10] - 0.020 m [5]	= 0.829 m (worst-case)
$(c.p.-c.m.)_z$	= 0.218 m - 1.270 m	= -1.052 m (worst-case)
C_D	= drag coefficient	= 2.2 along all axes
ρ_{Yelle}	= Yelle's atmospheric density [kg/m^3]	= f × ρ_{Adler}
V	= spacecraft velocity relative to Titan [m/s^2]	
A	= spacecraft projected area [10]	= 20.974 m^2 (worst-case, see Appendix)

Note: For this analysis, atmospheric effects were ignored above an altitude ≥ 3000 km, since no data is provided by Yelle's model for this region.

The atmospheric density was determined using Adler's equation for Yelle's model:

$$\rho_{Adler}(z) = 6.35\times10^{-6}\exp\left(-\frac{11400(z-76)}{T(z+2575)}\right) + 5.13\times10^{-7}\exp\left(-\frac{8030(z+429)}{T(z+2575)}\right) + 7.35\times10^{-5}\exp\left(-\frac{15000(z-44)}{T(z+2575)}\right) \ \text{g/cm}^3 \quad (3)$$

Adler's equation holds while z is between 800 and 3000 km. The mean temperature is T = 175 K, with a standard deviation of 10 K. This memo includes analysis of one-sided 0 sigma (T = 175 K, 50% confidence), 1.65 sigma (T = 191.5 K, 95% confidence), and 2.33 sigma (T = 198.3 K, 99% confidence).

The altitude and velocities are functions of the spacecraft flyby trajectory. Using 2-body orbital mechanics, a hyperbolic trajectory was computed from the position and velocity at Titan closest approach (TCA). Taking the time at TCA to be t = 0, positions and velocities were found using MATLAB tool to iterate and solve the respective equations. The radius of Titan is assumed to be 2575 km; subtracting this value from the position produces the altitude above Titan's surface.

At altitudes of ~1200 km and below, the values of ρ_{Adler} are less than ρ_{Yelle}. For flybys with TCA altitudes ≤ 1200 km the densities were multiplied by the factor below, to ensure that the more conservative of ρ_{Adler} and ρ_{Yelle} is always used:

$$f = \frac{\rho_{Yelle}(z = TCA, recommended)}{\rho_{Adler}(z = TCA, \sigma = 0)} > 1 \ [2] \qquad (4)$$

For the first Titan flyby, the factor f defined above is approximately 1.002 whereas for the 3rd and 43rd flybys, it is roughly equal to 1.046.

Target Motion Compensation (TMC) Torque

(i) Angular Acceleration for Nadir Pointing

Let us assume that the trajectory for all Titan flybys is hyperbolic, which is indeed a good assumption compared to the navigation data, the spacecraft is nadir pointed starting at time t = 0 where $r = r_0$, and $\theta = -\theta_0$, as shown in Figure 3 below. Since at any point corresponding to time t, the distance from the center of spacecraft to the center of Titan, r, is given by: $r = \frac{p}{1 + e\cos\theta}$,

then,

$$r_0 = \frac{p}{1 + e\cos\theta_0} \quad \text{and} \quad \theta_0 = Cos^{-1}\left[\frac{1}{e}\left(\frac{p}{r_0} - 1\right)\right] \tag{5}$$

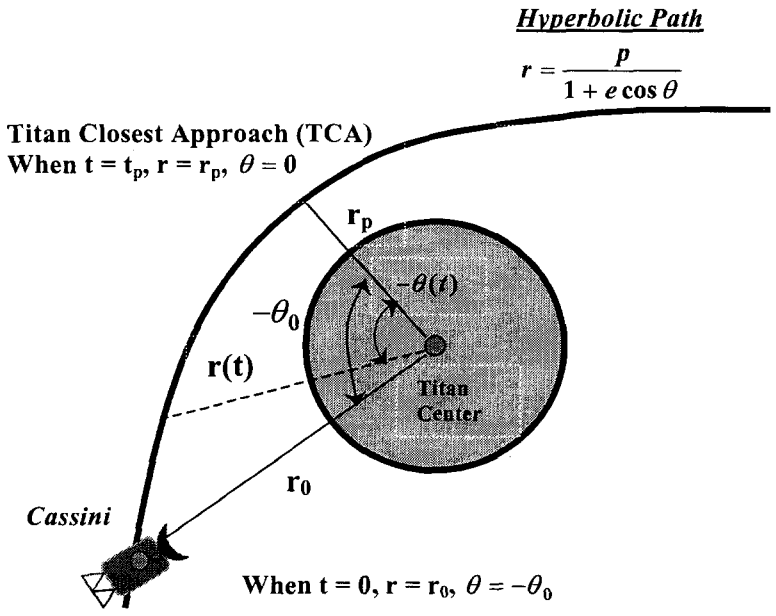

Figure 3 - Nadir pointing geometry

The angular rate is given by:

$$\dot{\theta} = \frac{h}{r^2} = \frac{h}{p^2}(1 + e\cos\theta)^2 \tag{6}$$

The angular acceleration is given by:

$$\ddot{\theta} = \frac{-2h^2 e}{p^4}\sin\theta(1 + e\cos\theta)^3 \tag{7}$$

The angular acceleration, $\ddot{\theta}$, is zero and changes sign at $\theta = 0$ (TCA), i.e., $\ddot{\theta} > 0$ when $\theta < 0$, and $\ddot{\theta} < 0$ when $\theta > 0$. Therefore, at the closest approach when atmospheric torque is a maximum, the TMC torque is luckily zero. The maximum of $\ddot{\theta}$ occurs at the angles of $\pm\theta_m$ where $0 < \theta_m < 90°$, and θ_m is given by:

$$\theta_m = Cos^{-1}\left(\frac{-1+\sqrt{1+48e^2}}{8e}\right) \tag{8}$$

where, the eccentricity $e = \frac{r_p V_p^2}{\mu_{Ti\tan}} - 1$ is ~15 for the 1200 km (first Titan flyby) and ~13 for 950 km flybys. This means that $\theta_m \approx Cos^{-1}\left(\frac{\sqrt{3}}{2}\right) = 30°$. The gravitational parameter of Titan (μ_{Titan}) is approximately 8977.97 km^3/s^2.

For $\theta = \pm\theta_m$, $r_m = \frac{p}{1+e\cos\theta_m} = \frac{8p}{7+\sqrt{1+48e^2}}$ (9)

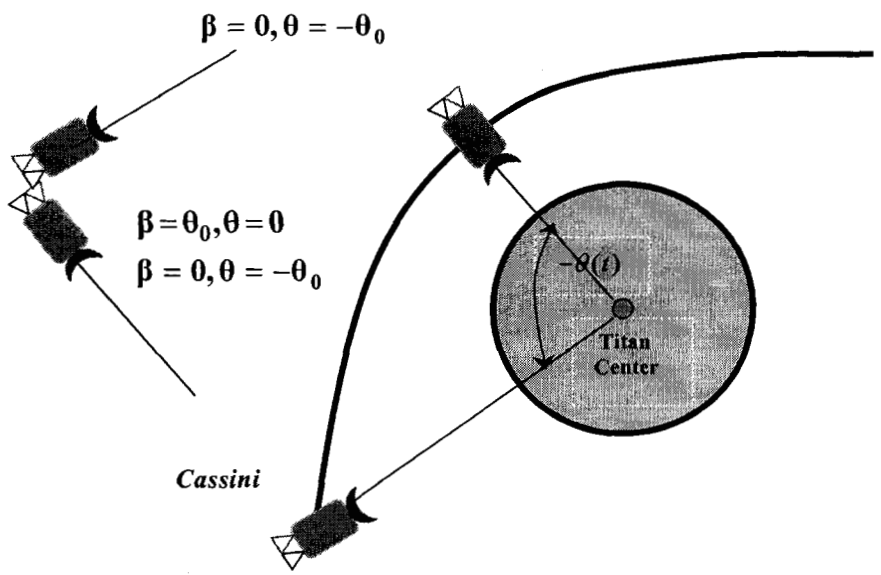

Figure 4 - Definition of the body angle β

Let $\beta = \theta + \theta_0$, as indicated in Figure 4. Then $\dot{\beta} = \dot{\theta}$, and $\dot{\beta} = \frac{h}{p^2}[1 + e\cos(\beta - \theta_0)]$. Then the TMC maximum angular acceleration and torque (in absolute value sense) are given by:

$$|\ddot{\beta}_{\max}| = \frac{2h^2\sqrt{2}}{(8p)^4}\left(7+\sqrt{1+48e^2}\right)^3\sqrt{8e^2-1+\sqrt{1+48e^2}} \tag{10}$$

$$|M_{\max}| = \frac{2I_{yy}h^2\sqrt{2}}{(8p)^4}\left(7+\sqrt{1+48e^2}\right)^3\sqrt{8e^2-1+\sqrt{1+48e^2}} \tag{11}$$

where h is the specific angular momentum of the orbit around Titan, p is the orbit semilatus rectum, e is the eccentricity, and I_{yy} is the spacecraft moment of inertia about the body Y-axis.

(ii) Angular Acceleration for Spotlight Pointing

Spotlight pointing occurs when the spacecraft is pointing at an interesting point on the surface of Titan. In a few of the Titan flybys, or at least one, the spacecraft may be spotlight pointed. It is assumed that the spotlight is located at a point that causes the spacecraft angular rate, as a result of spotlight pointing, to be a maximum. The angular rate is given by:

$$\dot{\varphi}_{\max} = \frac{h}{p} \cdot \frac{(1+e)^2 (p - \mathrm{Re} - R)}{p^2 + R(1+e)(R + \mathrm{Re} - 2p)} \tag{12}$$

where R is the Titan radius and is 2575 km and φ is defined in Figure 5 below.

The angular acceleration is given by:

$$\ddot{\varphi} = \frac{h^2}{p^3} \sin\theta (1 + e\cos\theta)^3 \times \frac{1}{\left\{p^2 + R(1+e\cos\theta)[R + (\mathrm{Re} - 2p)\cos\theta]\right\}^2} \times \left(\begin{array}{l} \{R(1+e\cos\theta) - 2e[(p - \mathrm{Re}) - R\cos\theta]\} \times \left\{p^2 + R(1+e\cos\theta)[R + (\mathrm{Re} - 2p)\cos\theta]\right\} + \\ R\{e[R + (\mathrm{Re} - 2p)\cos\theta] + (1 + e\cos\theta)(\mathrm{Re} - 2p)\} \times \{(1 + e\cos\theta)[(p - \mathrm{Re}) - R\cos\theta]\} \end{array} \right) \tag{13}$$

Note that if θ is negative, $\ddot{\varphi} > 0$, and vice versa. Also, note that at θ = φ = 0, $\ddot{\varphi} = 0$. Therefore, at the closest approach when atmospheric torque is a maximum, the TMC torque associated with spotlight pointing is luckily zero, once again. Figure 6 shows the plot of angular acceleration versus the angle θ for nadir and spotlight-pointed TMC. Note that both of the accelerations approach zero at TCA. Also, note the peak acceleration for nadir pointing occurs at ±30°.

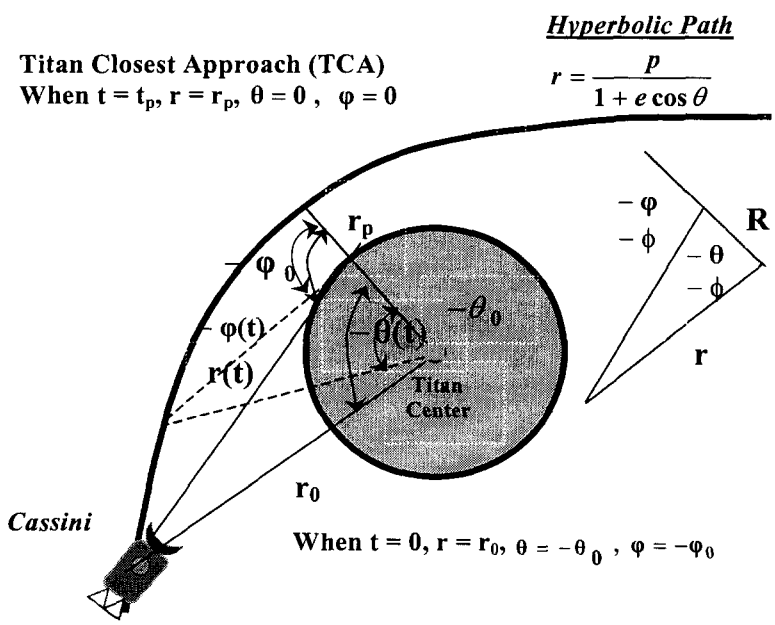

Figure 5 - Spotlight pointing geometry

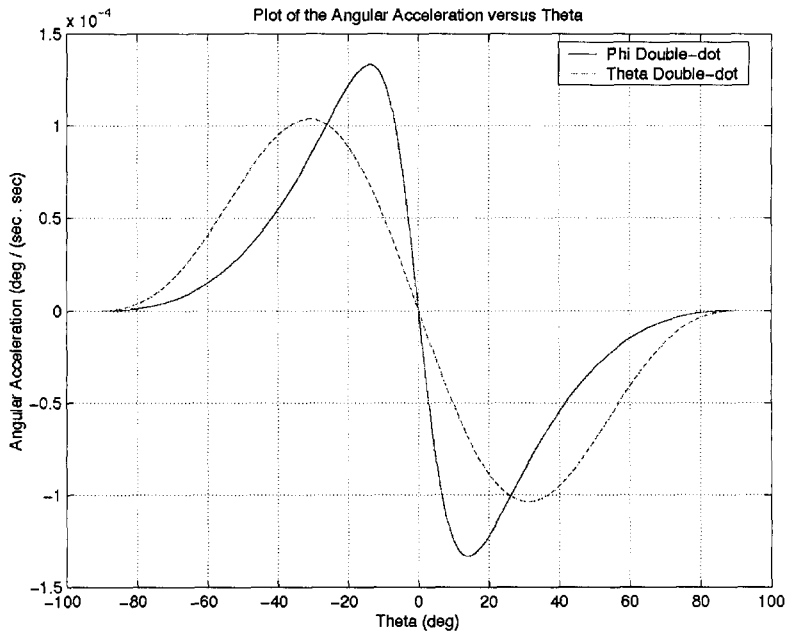

Figure 6 - Plot of angular acceleration versus the angle theta for nadir and spotlight-pointed TMC

Gravity Gradient Torque

The equations for worst-case gravity gradient torque are:

$$\left|T_{GG-y}\right| = \frac{3\mu_{TITAN}\left(I_{xx} - I_{zz}\right)}{2d^3} \quad \text{Nm} \tag{14}$$

$$\left|T_{GG-z}\right| = \frac{3\mu_{TITAN}\left(I_{yy} - I_{xx}\right)}{2d^3} \quad \text{Nm} \tag{15}$$

μ_{TITAN}	= gravitational parameter of Titan	= 8977.97 km^3/s^2
I_{xx}	= X moment of inertia	= 7540.6 kg-m^2 (Pre-), 7369.4 kg-m^2 (Post-Release)
I_{yy}	= Y moment of inertia	= 6899.4 kg-m^2 (Pre-), 6136.7 kg-m^2 (Post-Release)
I_{zz}	= Z moment of inertia	= 4441.2 kg-m^2 (Pre-), 3724.6 kg-m^2 (Post-Release)
d	= distance from spacecraft center of mass to Titan center (km)	

Note: The moments of inertia change after the probe is released. Current plans show that probe release occurs after the 2nd targeted flyby.

Radiation Torques

There are two radiation torques worth noting during Titan flybys. The first is torque due to solar radiation on the magnetometer boom:

$$\left|T_{SolRad-y}\right| = \left|\left(c.p._{MAG} - c.m.\right)_z\right| \times \frac{F_0}{cr^2} A_{MAG} \cos(\beta)\left[(1 + C_s)\cos(\beta) + \tfrac{2}{3} C_d\right] \quad \text{Nm} \tag{16}$$

$$|T_{SolRad-z}| = \left|(c.p._{MAG} - c.m.)_y\right| \times \frac{F_0}{cr^2} A_{MAG} \cos(\beta)\left[(1 + C_s)\cos(\beta) + \tfrac{2}{3} C_d\right] \quad \text{Nm} \qquad (17)$$

$(c.p._{MAG} - c.m.)_y$ = 6.50 m - 0.02 m		= 6.48 m (worst-case)
$(c.p._{MAG} - c.m.)_z$ = -0.69 m - 1.27 m		= -1.96 m (worst-case)
A_{MAG}	= magnetometer boom area	= 10 m × 0.48 m × 1.1 = 5.28 m^2
F_0	= solar constant	= 1353 W/m^2
c	= speed of light	= 2.998×10^8 m/s
r	= distance between sun and spacecraft	≈ 9.537 AU
C_s	= coefficient of specular reflection	≈ 0
C_d	= coefficient of diffuse reflection	≈ 0.06
β	= angle between incident ray and surface normal	≈ 0° (worst-case)

The other radiation torque considered is the RTG radiation torque, which is constant:

$$|T_{RTG-y}| = 0.30\times10^{-6} \quad \text{Nm} \qquad |T_{RTG-z}| = 3.21\times10^{-6} \quad \text{Nm} \qquad (18)$$

Total Torque at TCA

The total torque at TCA is the sum of the atmospheric drag, gravity gradient, and radiation torques (TMC torque is zero at TCA):

$$|T_y| = |T_{atm-y}| + |T_{GG-y}| + |T_{SolRad-y}| + |T_{RTG-y}| \quad \text{Nm} \qquad (19)$$

$$|T_z| = |T_{atm-z}| + |T_{GG-z}| + |T_{SolRad-z}| + |T_{RTG-z}| \quad \text{Nm} \qquad (20)$$

The worst-cases in this analysis are the 43rd and 44th targeted flybys with TCA altitude of 950 km and Titan-relative speed of 6.4 km/s.

Figure 7 depicts the sum of the atmospheric drag torque and the gravity gradient torque about Z-axis, for the first 950 km Titan flyby (the 3rd targeted flyby) using the recommended density model. The horizontal axis is the time with respect to TCA in seconds. Note that the atmospheric, as well as the gravity gradient torques peak rapidly within ±200 s. In fact, the torque at TCA is double the torque 1.5 min before and after TCA.

There are uncertainties associated with all terms in equations 1 and 2. The estimated (2σ) uncertainty in the atmospheric drag torque is computed to be about 30%. This means that the drag torque components must be increased by a factor of 1.30 when computing the control authority about Y and Z axes. Reference [10] is used to obtain both the projected area as well as the center of pressure location (see Appendix). This reference provides the data only for some viewing angles (all in X-Z plane). Besides, the main engine cover is not included. The impact of excluding the main engine cover is an increase in the projected area and a decrease in the moment arm (c.p. – c.m.) by approximately 10% resulting in a zero overall deterministic error.

The knowledge uncertainty of the spacecraft center of mass is better than ±5 cm.

The attitude control torque required to maintain the commanded thruster controller deadband is approximately 0.05 Nm. This quantity must also be added to the total torque to be overcome by thrusters during Titan flybys. In addition, if there are Science slews near TCA, part of the thruster control authority must be used to accelerate or decelerate the spacecraft about the slew axis (or axes). These Science slews must be designed in such a way that adequate controllability margins about all axes (specially Y and Z axes) are maintained. A project consensus on what constitutes the adequate margin is also needed.

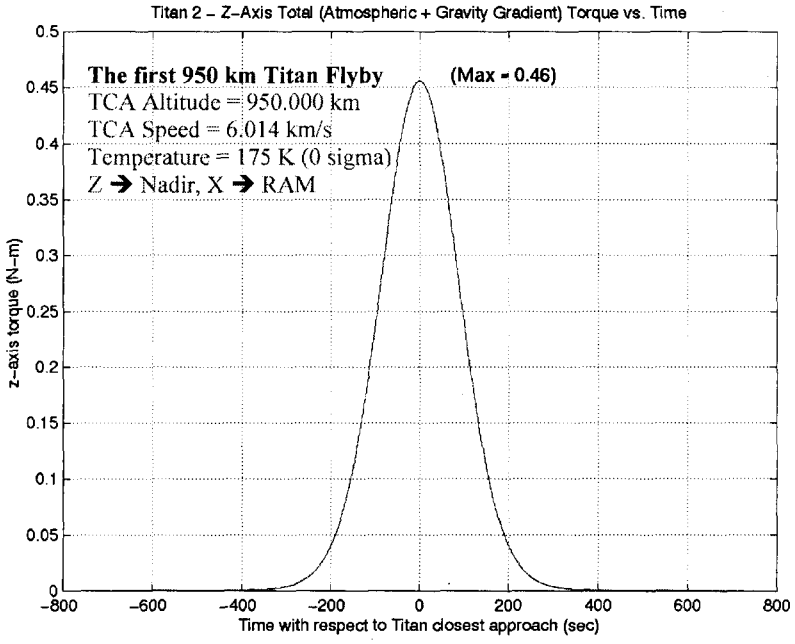

Figure 7 - Atmospheric plus gravity gradient torque about Z-axis for the first 950 km flyby

Per-Axis Thruster Control Authority

In this section, some analytical expressions for the spacecraft per-axis thruster control authority are derived. We shall assume that the thrust magnitude of all thrusters (Y_1, Y_2, Y_3, Y_4, Z_1, Z_2, Z_3, Z_4) is F (N). F is the A-branch (primary cluster) thrusters' thrust magnitude and varies from 1.0 N at the beginning of mission (BOM) and immediately after the recharge to 0.5 N at the end of mission (EOM). In reality, the thrust force is not the same for of all thrusters and varies slightly from one thruster to another. In fact, the knowledge uncertainties of the thrust produced by these thrusters include a ±7% pulse-to-pulse and ±5% thruster-to-thruster variation [1]. The angular misalignment between the actual thrust vector and the spacecraft axes is below 1°, and the locations of the thruster nozzle centers are known to be better than 1.1 cm [1].

The following nomenclature is used in this section.

Nomenclature:

D_i (i = 1 … 4)	=	Duty cycle of a Z-facing thruster Z_i. Obviously, $0 \leq D_i \leq 1$.
F	=	Thrust force of all RCS thrusters.
M_x , M_y, M_z	=	Thruster-provided torque about spacecraft X, Y, and Z axes.

By examining Table (1) below, it is realized that CM_y is always positive after magnetometer boom is deployed, and CM_x changes sign immediately after probe release. Furthermore, the quantities $l_y(CM_x) \pm l_x(CM_y)$ have the same sign as CM_x.

The separation of the approximately 350-kg Huygens probe from Cassini orbiter will cause a large shift (as large as 15 cm) in the X-component of the orbiter's center of mass, as indicated in Table (1).

Table 1 – The X and Y components of center of mass in various mission phases

Mission Phase	CM_x *(m)*	CM_y *(m)*	Sign of $(l_xCM_y + l_yCM_x)$	Sign of $(l_xCM_y - l_yCM_x)$
Launch, BOM	-0.03	-0.01	Negative	Positive
Current	-0.03	+0.01	Negative	Positive
Pre-Probe Release (1st Titan flyby)	-0.04	+0.02	Negative	Positive
Post-Probe Release (right after release)	+0.11	+0.02	Positive	Negative
EOM	+0.14	+0.06	Positive	Negative

First we shall consider the torque authority about Z-axis, indicated by μ_z where μ_z is a dimensionless positive number between 0 and 1. The torque about Z-axis is generated by firing two diagonally opposite Y-facing thrusters (see Figure 2). If the largest possible j-axis torque (j = x, y, z) is denoted by M_j^{Peak}, then,

$$M_z^{Peak} = 2Fl_x \qquad \text{Nm} \tag{21}$$

This equation is independent of the spacecraft center of mass location. The control authority about the Z-axis, μ_z is defined as:

$$\mu_z = \frac{M_z}{M_z^{Peak}}$$

Therefore, it is easy to realize the controllability region for torques about Z-axis (see Figure 8).

Now, let's consider torques bout X and Y axes, i.e. when Z-facing thrusters are fired. We define the control authority about X and Y axes as $\mu_x = \dfrac{M_x}{M_x^{Peak}}$ and $\mu_y = \dfrac{M_y}{M_y^{Peak}}$, respectively.

Table (2) below summarizes the RCS thruster firing logic. The Cassini flight software does not allow the diagonally opposite Z-facing thrusters to fire simultaneously because this condition is undesirable. It leads to an unwanted ΔV and additional hydrazine consumption while generating very small net torque. This means the sum of duty cycles of the diagonally opposite Z-facing thrusters must be less than or equal to 100%, e.g. $D_1 + D_3 \leq 1$.

Table 2 – Possible cases for Z-facing thruster firings – Note: $0 \leq D_i \leq 1$ (i = 1, 2, 3, 4)

Case	Generated Torque about X-axis	Generated Torque about Y-axis	Z-Facing Thrusters to Fire	Duty Cycle of Z-Facing Thrusters
1	$M_x > 0$	$M_y > 0$	Z_1, Z_3, Z_4	D_1, D_3, D_4
2	$M_x > 0$	$M_y < 0$	Z_2, Z_3, Z_4	D_2, D_3, D_4
3	$M_x < 0$	$M_y > 0$	Z_1, Z_2, Z_4	D_1, D_2, D_4
4	$M_x < 0$	$M_y < 0$	Z_1, Z_2, Z_3	D_1, D_2, D_3

Close examination of Figure (2) and table (2) reveals that there exists an interaction between X- and Y-axis control authorities. For each of the four cases indicated in Table (2), the control authority about X and Y axes (μ_x and μ_y) are subsequently derived (see equations 22 though 29 below).

Case(1): $M_x > 0$ and $M_y > 0$.
Thrusters Z_1, Z_3, and Z_4 are firing with duty cycles D_1, D_3, and D_4, respectively.

$$M_x = FD_3(l_y + CM_y) + FD_4(l_y + CM_y) - FD_1(l_y - CM_y)$$
$$M_x^{Peak} = 2F(l_y + CM_y)$$
$$\mu_x = \frac{M_x}{M_x^{Peak}} = \frac{(D_3 + D_4)(l_y + CM_y) - D_1(l_y - CM_y)}{2(l_y + CM_y)}$$
$$\mu_x = \frac{D_3 + D_4}{2} - \frac{D_1}{2}\left(\frac{l_y - CM_y}{l_y + CM_y}\right) \quad , \quad [0 \le \mu_x \le 1] \qquad (22)$$

and,

$$M_y = FD_1(l_x - CM_x) + FD_4(l_x - CM_x) - FD_3(l_x + CM_x)$$
$$M_y^{Peak} = 2F(l_x - CM_x)$$
$$\mu_y = \frac{M_y}{M_y^{Peak}} = \frac{(D_1 + D_4)(l_x - CM_x) - D_3(l_x + CM_x)}{2(l_x - CM_x)}$$
$$\mu_y = \frac{D_1 + D_4}{2} - \frac{D_3}{2}\left(\frac{l_x + CM_x}{l_x - CMx}\right) \quad , \quad [0 \le \mu_y \le 1] \qquad (23)$$

Case(2): $M_x > 0$ and $M_y < 0$.
Thrusters Z_2, Z_3, and Z_4 are firing with duty cycles D_2, D_3, and D_4, respectively.

$$M_x = FD_3(l_y + CM_y) + FD_4(l_y + CM_y) - FD_2(l_y - CM_y)$$
$$M_x^{Peak} = 2F(l_y + CM_y)$$
$$\mu_x = \frac{M_x}{M_x^{Peak}} = \frac{(D_3 + D_4)(l_y + CM_y) - D_2(l_y - CM_y)}{2(l_y + CM_y)}$$
$$\mu_x = \frac{D_3 + D_4}{2} - \frac{D_2}{2}\left(\frac{l_y - CM_y}{l_y + CM_y}\right) \quad , \quad [0 \le \mu_x \le 1] \qquad (24)$$

and,

$$M_y = -FD_2(l_x + CM_x) + FD_4(l_x - CM_x) - FD_3(l_x + CM_x)$$
$$M_y^{Peak} = -2F(l_x + CM_x)$$
$$\mu_y = \frac{M_y}{M_y^{Peak}} = \frac{D_4(l_x - CM_x) - (D_2 + D_3)(l_x + CM_x)}{-2(l_x + CM_x)}$$
$$\mu_y = \frac{D_2 + D_3}{2} - \frac{D_4}{2}\left(\frac{l_x - CM_x}{l_x + CMx}\right) \quad , \quad [0 \le \mu_y \le 1] \qquad (25)$$

Case(3): $M_x < 0$ and $M_y > 0$.
Thrusters Z_1, Z_2, and Z_4 are firing with duty cycles D_1, D_2, and D_4, respectively.

$$M_x = -FD_1(l_y - CM_y) - FD_2(l_y - CM_y) + FD_4(l_y + CM_y)$$
$$M_x^{Peak} = -2F(l_y - CM_y)$$
$$\mu_x = \frac{M_x}{M_x^{Peak}} = \frac{D_4(l_y + CM_y) - (D_1 + D_2)(l_y - CM_y)}{-2(l_y - CM_y)}$$
$$\mu_x = \frac{D_1 + D_2}{2} - \frac{D_4}{2}\left(\frac{l_y + CM_y}{l_y - CM_y}\right) \quad , \quad [0 \le \mu_x \le 1] \tag{26}$$

and,

$$M_y = FD_1(l_x - CM_x) + FD_4(l_x - CM_x) - FD_2(l_x + CM_x)$$
$$M_y^{Peak} = 2F(l_x - CM_x)$$
$$\mu_y = \frac{M_y}{M_y^{Peak}} = \frac{(D_1 + D_4)(l_x - CM_x) - D_2(l_x + CM_x)}{2(l_x - CM_x)}$$
$$\mu_y = \frac{D_1 + D_4}{2} - \frac{D_2}{2}\left(\frac{l_x + CM_x}{l_x - CMx}\right) \quad , \quad [0 \le \mu_y \le 1] \tag{27}$$

Case(4): $M_x < 0$ and $M_y < 0$.
Thrusters Z_1, Z_2, and Z_3 are firing with duty cycles D_1, D_2, and D_3, respectively.

$$M_x = -FD_1(l_y - CM_y) - FD_2(l_y - CM_y) + FD_3(l_y + CM_y)$$
$$M_x^{Peak} = -2F(l_y - CM_y)$$
$$\mu_x = \frac{M_x}{M_x^{Peak}} = \frac{D_3(l_y + CM_y) - (D_1 + D_2)(l_y - CM_y)}{-2(l_y - CM_y)}$$
$$\mu_x = \frac{D_1 + D_2}{2} - \frac{D_3}{2}\left(\frac{l_y + CM_y}{l_y - CM_y}\right) \quad , \quad [0 \le \mu_x \le 1] \tag{28}$$

and,

$$M_y = -FD_2(l_x + CM_x) - FD_3(l_x + CM_x) + FD_1(l_x - CM_x)$$
$$M_y^{Peak} = -2F(l_x + CM_x)$$
$$\mu_y = \frac{M_y}{M_y^{Peak}} = \frac{D_1(l_x - CM_x) - (D_2 + D_3)(l_x + CM_x)}{-2(l_x + CM_x)}$$
$$\mu_y = \frac{D_2 + D_3}{2} - \frac{D_1}{2}\left(\frac{l_x - CM_x}{l_x + CMx}\right) \quad , \quad [0 \le \mu_y \le 1] \tag{29}$$

First adding (23) to (22) and then subtracting (23) from (22) yields the following system of linear equations:

$$\begin{cases} D_1\left(\dfrac{CM_y}{l_y + CM_y}\right) - D_3\left(\dfrac{CM_x}{l_x - CM_x}\right) = \mu_x + \mu_y - D_4 \\ -D_1\left(\dfrac{l_y}{l_y + CM_y}\right) + D_3\left(\dfrac{l_x}{l_x - CM_x}\right) = \mu_x - \mu_y \end{cases} \tag{30}$$

The values of l_x, l_y, CM_x, CM_y are such that $l_xCM_y - l_yCM_x \neq 0$. This quantity is positive for pre-probe release and negative for post-probe release conditions.

The solution to the system of equations (30) is:

$$D_1 = (l_y + CM_y)\frac{l_x(\mu_x + \mu_y - D_4) + CM_x(\mu_x - \mu_y)}{l_x CM_y - l_y CM_x}$$

$$D_3 = (l_x - CM_x)\frac{l_y(\mu_x + \mu_y - D_4) + CM_y(\mu_x - \mu_y)}{l_x CM_y - l_y CM_x}$$

Hence the sum $D_1 + D_3$ is:

$$D_1 + D_3 = \mu_x\left[\frac{2l_x(l_y + CM_y)}{l_x CM_y - l_y CM_x}\right] + \mu_y\left[\frac{2l_y(l_x - CM_x)}{l_x CM_y - l_y CM_x}\right] - D_4\left[1 + \frac{2l_x l_y}{l_x CM_y - l_y CM_x}\right] \tag{31}$$

Now, let:

$$K_{11} = \frac{2l_x(l_y + CM_y)}{l_x CM_y - l_y CM_x}$$

$$K_{12} = \frac{2l_y(l_x - CM_x)}{l_x CM_y - l_y CM_x} \qquad \text{(Note that: } l_x CM_y - l_y CM_x \neq 0\text{)}$$

$$K_{13} = 1 + \frac{2l_x l_y}{l_x CM_y - l_y CM_x}$$

Based on the sign of CM_x, two cases should now be distinguished:

Case 1.A: Pre-probe release scenario for which: CMx = -0.04 m, $l_x CM_y - l_y CM_x > 0$, and K_{11}, K_{12}, and K_{13} are all positive.

Case 1.B: Post-probe release scenario for which: CMx = +0.11 m, $l_x CM_y - l_y CM_x < 0$, and K_{11}, K_{12}, and K_{13} are all negative.

Since $0 \leq D_1 + D_3 \leq 1$ and $0 \leq D_4 \leq 1$, $0 \leq K_{11}\mu_x + K_{12}\mu_y - K_{13}D_4 \leq 1$. Thus,

$$K_{13}D_4 \leq K_{11}\mu_x + K_{12}\mu_y \leq 1 + K_{13}D_4 \tag{32}$$

- **<u>Case 1.A ($K_{11} > 0$, $K_{12} > 0$, and $K_{13} > 0$):</u>**

The condition $0 \leq D_4 \leq 1$ implies $0 \leq K_{13}D_4 \leq K_{13}$. Also, $1 \leq 1 + K_{13}D_4 \leq 1 + K_{13}$. Combining these inequalities with (32) yields:

$$0 \leq K_{13}D_4 \leq K_{11}\mu_x + K_{12}\mu_y \leq 1 + K_{13}D_4 \leq 1 + K_{13} \tag{33}$$

From the above combined inequalities, it can be deduced that: $K_{11}\mu_x + K_{12}\mu_y \leq 1 + K_{13}$. Therefore,

$$\frac{\mu_x}{A_1} + \frac{\mu_y}{B_1} \leq 1 \tag{34}$$

where,

$$A_1 = \frac{1 + K_{13}}{K_{11}} = 1 - \frac{l_y CM_x}{l_x(l_y + CM_y)} \approx 1.03 \text{ and } B_1 = \frac{1 + K_{13}}{K_{12}} = 1 + \frac{l_x CM_y}{l_y(l_x - CM_x)} \approx 1.01.$$

Figure 9 captures the region indicated by equation (34) above. The angle θ_1 in the figure is computed as:

$$\theta_1 = Tan^{-1}\left(\frac{B_1}{A_1}\right) = Tan^{-1}\left(\frac{1+\frac{CM_y}{l_y}}{1-\frac{CM_x}{l_{x\approx}}}\right) \approx 44.4^\circ \tag{35}$$

Some checking observations can be made here:

- When $D_1 = D_4 = 1$ and $D_3 = 0$, then $\mu_y = 1$. Both equations (22) and (34) yield $\mu_x = \frac{CM_y}{l_y + CM_y} = 0.0125$.
- When $D_3 = D_4 = 1$ and $D_1 = 0$, then $\mu_x = 1$. Both equations (23) and (34) yield $\mu_y = \frac{-CM_x}{l_x - CM_x} > 0$ because $CM_x < 0$.

- **<u>Case 1.B ($K_{11} < 0$, $K_{12} < 0$, and $K_{13} < 0$):</u>**

The condition $0 \le D_4 \le 1$ implies $K_{13} \le K_{13}D_4 \le 0$. Also, $1 + K_{13} \le 1 + K_{13}D_4 \le 1$. Combining these inequalities with (32) yields:

$$0 \ge K_{11}\mu_x + K_{12}\mu_y \ge K_{13}D_4 \le K_{13} \tag{36}$$

Therefore,

$$\frac{\mu_x}{A'_1} + \frac{\mu_y}{B'_1} \le 1 \tag{37}$$

where,

$$A'_1 = \frac{K_{13}}{K_{11}} = \frac{1}{2}\left[1 + \left(\frac{l_y}{l_x}\right)\left(\frac{l_x - CM_x}{l_y + CM_y}\right)\right] \approx 0.95 < 1 \text{ and } B'_1 = \frac{K_{13}}{K_{12}} = \frac{1}{2}\left[1 + \left(\frac{l_x}{l_y}\right)\left(\frac{l_y + CM_y}{l_x - CM_x}\right)\right] \approx 1.06.$$

Note that both A'_1 and B'_1 are positive because they are ratios of two negative numbers.

Figure 10 captures the region indicated by equation (37) above. The angle θ'_1 in the figure is computed as:

$$\theta'_1 = Tan^{-1}\left(\frac{B'_1}{A'_1}\right) = Tan^{-1}\left(\frac{1+\frac{CM_y}{l_y}}{1-\frac{CM_x}{l_{x\approx}}}\right) \approx 48.0^\circ \tag{38}$$

Some checking observations can be made here:

- When $D_1 = D_4 = 1$ and $D_3 = 0$, then $\mu_y = 1$. Equation (22) yields $\mu_x = \frac{CM_y}{l_y + CM_y} = 0.0125$. However, equation (37) yields $\mu_x = \frac{l_x CM_y + l_y CM_x}{2l_x(l_y + CM_y)} \approx 0.05 > \frac{CM_y}{l_y + CM_y}$.
- When $D_3 = D_4 = 1$ and $D_1 = 0$, then $\mu_x = 1$. Both equations (23) and (37) yield negative numbers. This is because 100% authority about x-axis is not feasible.

Now, some other useful inequalities can be derived when combining the condition of $0 \le D_1 + D_3 \le 1$ and the second part of the system of equations given by (30), i.e. $-D_1\left(\frac{l_y}{l_y + CM_y}\right) + D_3\left(\frac{l_x}{l_x - CM_x}\right) = \mu_x - \mu_y$.

These inequalities are as follows:

$\mu_y \le \mu_x + E_1$ where $E_1 = \dfrac{l_y}{l_y + CM_y} \approx 0.99$, and

$\mu_y \ge \mu_x - C_1$ where $C_1 = \dfrac{l_x}{l_x - CM_x} \approx 0.97$.

Furthermore, the following useful results can easily be proven:

(i) $A_1 (B_1 + C_1) = B_1 (A_1 + E_1) = A_1 + B_1$.

(ii) $C_1 > A'_1$.

The key parameters for cases 1.A and 1.B are summarized in Table (3).

Table 3 – Key parameters for Cases 1.A and 1.B

Case (1.A)	Case (1.B)
Pre-probe release scenario for which: CMx = -0.04 m $l_xCM_y - l_yCM_x > 0$ K_{11}, K_{12}, and K_{13} are all positive	Post-probe release scenario for which: CMx = +0.11 m $l_xCM_y - l_yCM_x < 0$ K_{11}, K_{12}, and K_{13} are all negative
$A_1 = 1 - \dfrac{l_y CM_x}{l_x(l_y + CM_y)} \approx 1.03 > 1$ $B_1 = 1 + \dfrac{l_x CM_y}{l_y(l_x - CM_x)} \approx 1.01 > 1$ $C_1 = \dfrac{l_x}{l_x - CM_x} \approx 0.97 < 1$ $E_1 = \dfrac{l_y}{l_y + CM_y} \approx 0.99 < 1$ $\theta_1 = Tan^{-1}\left(\dfrac{1 + \frac{CM_y}{l_y}}{1 - \frac{CM_x}{l_{x\approx}}}\right) \approx 44.4°$ $\mu_{x1} = \dfrac{A_1(B_1 + C_1)}{A_1 + B_1} = 1$ $\mu_{y1} = \dfrac{B_1(A_1 - C_1)}{A_1 + B_1} = \dfrac{-CM_x}{l_x - CM_x} \approx 0.03$ $\mu_{x2} = \dfrac{A_1(B_1 - E_1)}{A_1 + B_1} = \dfrac{CM_y}{l_y + CM_y} = 0.0125$ $\mu_{y2} = \dfrac{B_1(A_1 + E_1)}{A_1 + B_1} = 1$	$A'_1 = \dfrac{1}{2}\left[1 + \left(\dfrac{l_y}{l_x}\right)\left(\dfrac{l_x - CM_x}{l_y + CM_y}\right)\right] \approx 0.95 < 1$ $B'_1 = \dfrac{1}{2}\left[1 + \left(\dfrac{l_x}{l_y}\right)\left(\dfrac{l_y + CM_y}{l_x - CM_x}\right)\right] \approx 1.06 > 1$ $C_1 = \dfrac{l_x}{l_x - CM_x} \approx 0.97 < 1$ $E_1 = \dfrac{l_y}{l_y + CM_y} \approx 0.99 < 1$ $\theta'_1 = Tan^{-1}\left(\dfrac{1 + \frac{CM_y}{l_y}}{1 - \frac{CM_x}{l_{x\approx}}}\right) \approx 48.0°$ $\mu'_{x2} = \dfrac{A'_1(B'_1 - E_1)}{A'_1 + B'_1} = \dfrac{2 + \frac{1}{2}\left(\frac{CM_y}{l_y} - \frac{CM_x}{l_x}\right)}{2 + \frac{CM_y}{l_y} - \frac{CM_x}{l_x}} - \dfrac{1}{1 + \frac{CM_y}{l_y}} \approx 0.03$ $\mu'_{y2} = \dfrac{B'_1(A'_1 + E_1)}{A'_1 + B'_1} = \dfrac{2 + \frac{1}{2}\left(\frac{CM_y}{l_y} - \frac{CM_x}{l_x}\right)}{2 + \frac{CM_y}{l_y} - \frac{CM_x}{l_x}} \approx 1.02 > 1$
Maximum torque authority of 100% exists about both X and Y axes.	Maximum torque authority of 100% exists only about Y-axis and not X-axis.

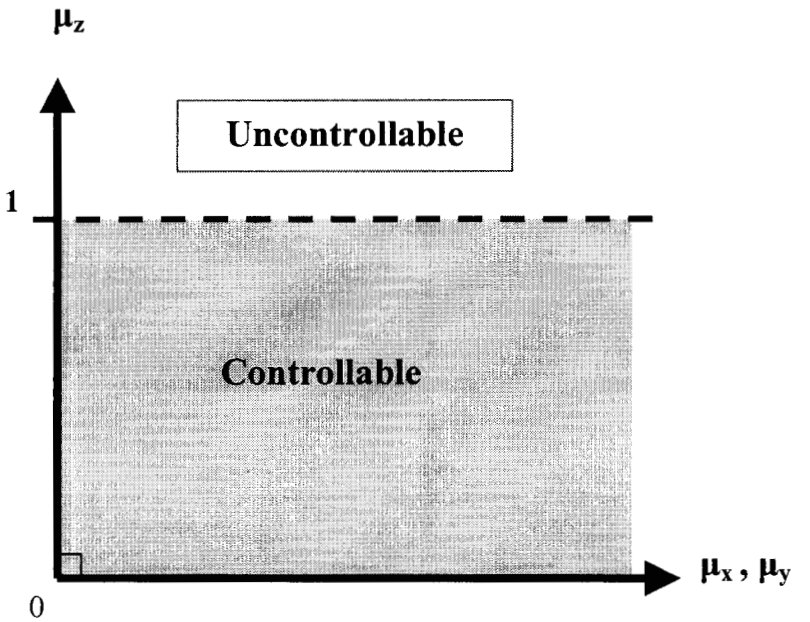

Figure 8 - Control authority about Z-axis

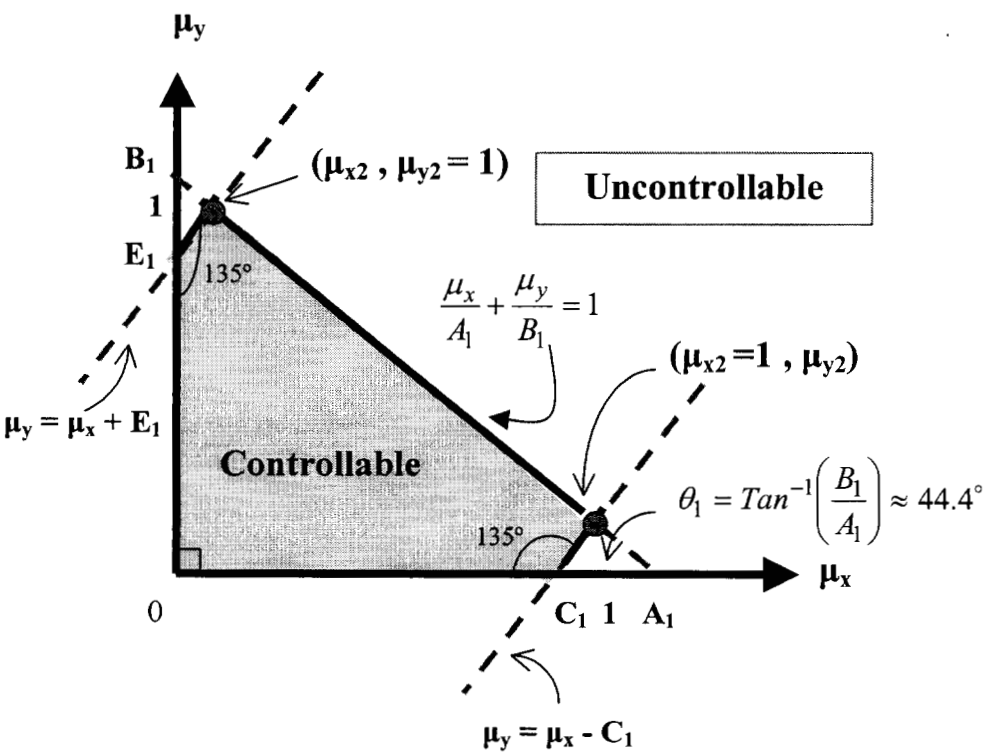

Figure 9 - Controllable region for Case 1.A with pre-probe release center of mass

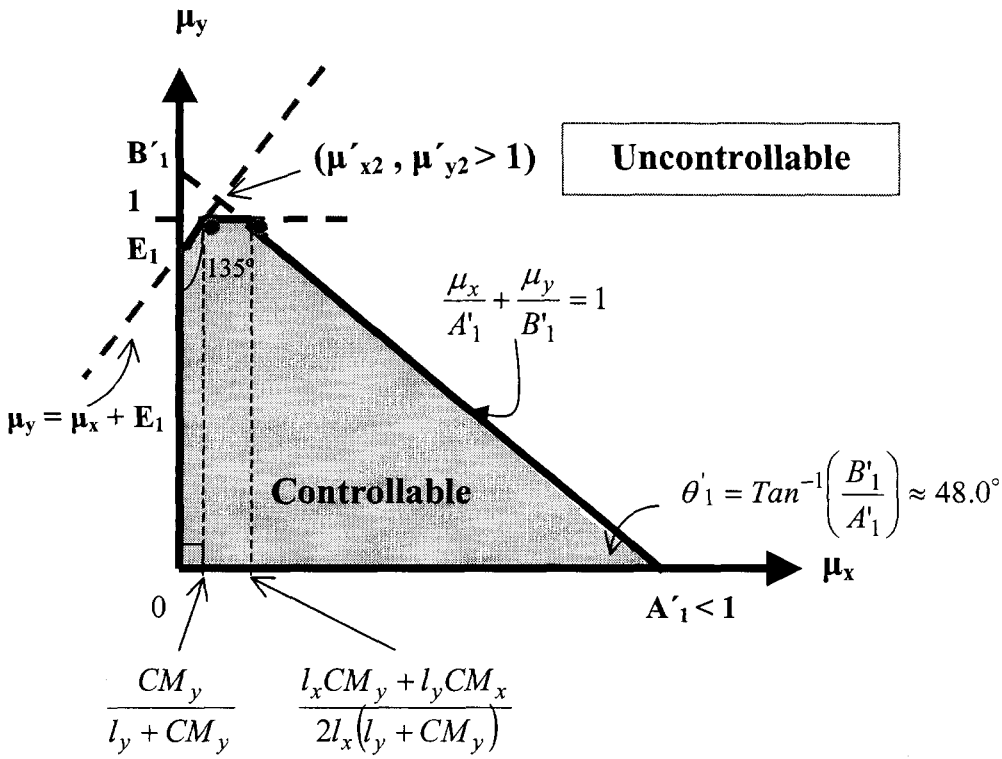

Figure 10 - Controllable region for Case 1.B with post-probe release center of mass

The remaining cases (2.A, 2.B, 3.A, 3.B, 4.A, and 4.B) lead to similar controllability diagrams with minor variations. Analytical expressions are developed for the boundaries of these controllability regions; however, these expressions are not presented in this paper. Instead, the MATLAB-generated rough geometric representation of these regions are depicted in Figure 11C-H.

Based on the close examination of all cases, a more conservative model is adopted (see Figure 12) in which the control authority about the X and Y axes is cut to 90%.

Table (4) shows the total torque exerted on the spacecraft for 3 different Titan flybys, 1st, 3rd, and 43rd.

Table 4 – Total torque for 3 key Titan flybys using recommended density model (50% Confidence)

Targeted Flyby No.	TCA Altitude *(km)*	TCA Titan-Relative Velocity *(km/s)*	Max Torque about Y-Axis *(Nm)*	Max Torque about Z-Axis *(Nm)*	Thrust Force *(N)*	(CM_x, CM_y) *(m)*
1	1200	6.1	0.02	0.02	~0.69	(-0.04,0.02)
3	950	6.0	0.59	0.46	~0.65	(0.11,0.04)
43	950	6.4	0.67	0.53	~0.50	(0.14,0.06)

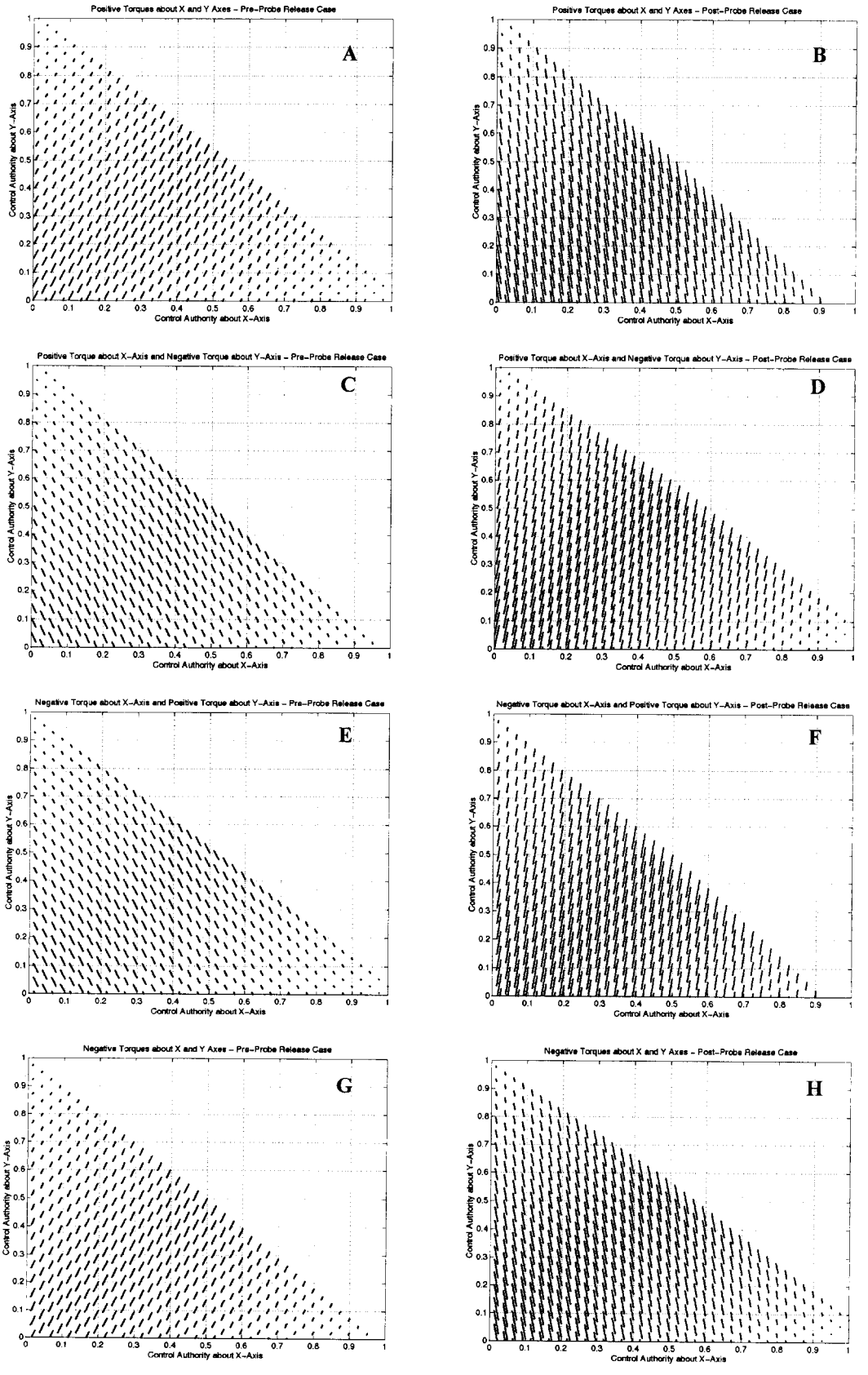

Figure 11A-H - The control authority region for all cases

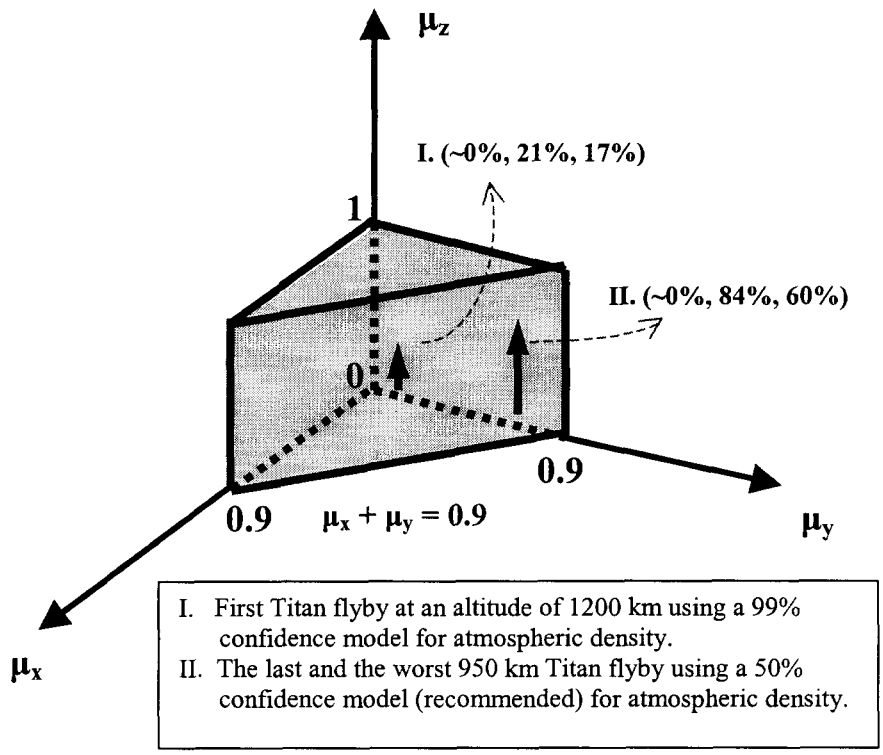

Figure 12 – The more conservative 3-D controllability diagram

Tables 5A, 5B, and 5C summarize the maximum torque about Y and Z-axes experienced by the spacecraft at TCA using three different density models (50%, 95%, and 99%) for the three selected targeted flybys. The worst peak torque about the Y and Z axes are also listed along with the computed control authorities about these axes. The worst peak torque about Y-axis is the largest of $2F(l_x \pm CM_x)$ depending on CM_x value.

Table 5A – Control authority about Y and Z axes for 1st targeted Titan flyby at 3 confidence levels

% Confidence (One-Sided σ)	Max Torque about Y-Axis *(Nm)*	Max Torque about Z-Axis *(Nm)*	Worst Peak Torque about Y-Axis *(Nm)*	Worst Peak Torque about Z-Axis *(Nm)*	μ_y (%)	μ_z (%)
50%	0.02	0.02	1.65	1.70	1	1
95%	0.12	0.10	1.65	1.70	7	6
99%	0.23	0.18	1.65	1.70	**14**	**11**

Table 5B – Control authority about Y and Z axes for 3rd targeted Titan flyby at 3 confidence levels

% Confidence (One-Sided σ)	Max Torque about Y-Axis *(Nm)*	Max Torque about Z-Axis *(Nm)*	Worst Peak Torque about Y-Axis *(Nm)*	Worst Peak Torque about Z-Axis *(Nm)*	μ_y (%)	μ_z (%)
50%	0.59	0.46	1.46	1.60	40	29
95%	2.41	1.90	1.46	1.60	**165**	**119**
99%	4.05	3.19	1.46	1.60	**277**	**199**

Table 5C – Control authority about Y and Z axes for 43rd targeted Titan flyby at 3 confidence levels

% Confidence (One-Sided σ)	Max Torque about Y-Axis *(Nm)*	Max Torque about Z-Axis *(Nm)*	Worst Peak Torque about Y-Axis *(Nm)*	Worst Peak Torque about Z-Axis *(Nm)*	μ_y (%)	μ_z (%)
50%	0.67	0.53	1.09	1.23	**61**	**43**
95%	2.75	2.18	1.09	1.23	**252**	**177**
99%	4.60	3.63	1.09	1.23	**422**	**295**

Figure 12 captures two Titan flyby scenarios: the first (1200 km) flyby using the 99% confidence model and the 43rd (950 km) flyby using the recommended model associated with the 50% confidence. The torques are first multiplied by a factor of 1.30 (to account for the 2σ uncertainty in atmospheric drag torque) and added by 0.05 Nm (attitude control torque). The result is plotted in Figure 12 (indicated by the two vertical arrows).

Conclusion

Figure 12 indicates that if the recommended Yelle Titan atmospheric density model is to be used to compute the atmospheric drag torque on Cassini during the worst low-altitude Titan flyby, there is still more than 6% margin for torque authority about Y-axis and a 40% margin for torque authority about Z-axis. This includes a 2σ estimated uncertainty in drag torque and the attitude control torque. Thus, it is ensured that Cassini, this largest and most sophisticated outer planet spacecraft ever built, will not tumble out of control at TCA during all low-altitude targeted flybys. In addition, there is more than adequate per-axis control authority margin for the first Titan flyby.

Currently the minimum Titan flyby altitude (950 km) is chosen to ensure that the spacecraft will be able to maintain attitude control while under the influence of atmospheric drag. In order to ensure that the first low (950 km) flyby of Titan is safe, measurements must be made of earlier, higher targeted flybys of Titan to determine the measured density of the Titan atmosphere. The purpose of such work is to ensure that the model upon which safety analyses was based is accurate, or at least conservative with respect to the actual atmospheric profile. After the first targeted flyby, the INMS team shall reduce and analyze the data necessary to compute the measured atmospheric density during the flyby. At the same time, Attitude and Articulation Control Subsystem (AACS) team (including the author of this paper) shall study the thruster telemetry during the first Titan flyby and derive the external torques about the X, Y, and Z axes from the Titan atmosphere as a function of time around closest approach. In addition, the spacecraft Thermal Control team shall study the thermal response of the spacecraft during the first Titan flyby and assess the safety of lowering the flyby altitude to 950 km.

After receiving these deliveries, Mission Planning will attempt to reconcile the AACS and INMS analyses. The density profile from INMS will be processed to compute the predicted torques about the X, Y, and Z axes for the attitude profile during the first Titan flyby and the corresponding INMS-derived torques will be compared to the AACS-derived set.

Appendix

Figure 13 below is part of the document[10] that provides the spacecraft projected area and center of pressure. This document provides limited data only for some viewing angles inside the spacecraft X-Z plane. Besides, the main engine cover is not included.

The projected area plots are created from the Cassini Geomod solid model mass properties database (in 1992) using a software that is specifically developed for this task.

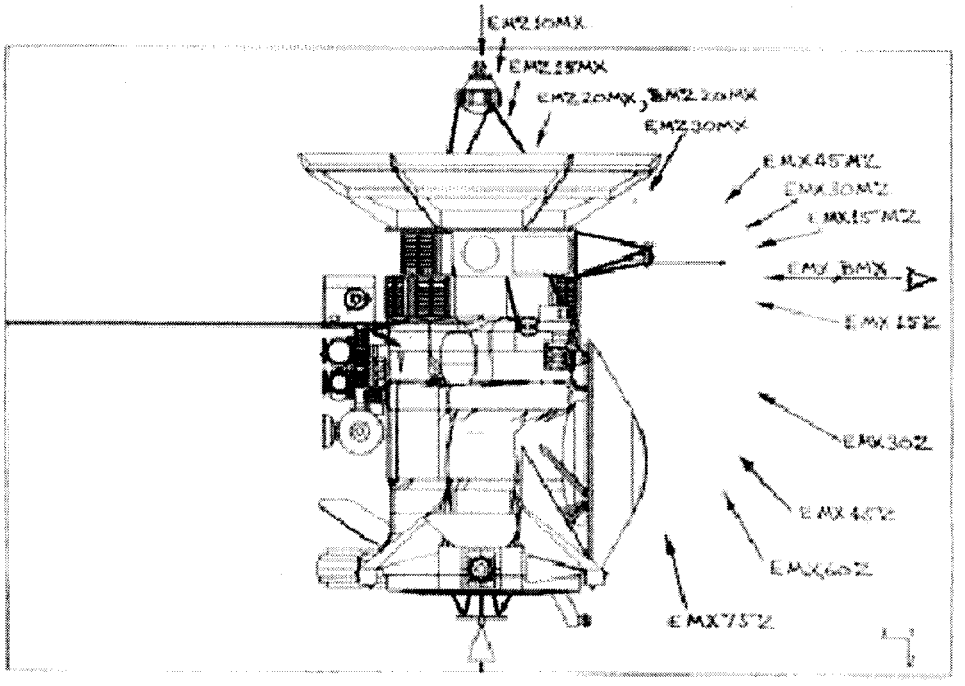

Figure 13 - Cassini projected area plot [10]. Note: Main Engine cover is not included

Naming Code: "E" stands for "End of Mission (EOM)" and "M" for "Minus".
For example, EMX30MZ refers to EOM configuration looking along a direction associated with the rotated –X body axis towards –Z body axis by 30°.

Acknowledgments

The research was carried out by the Jet Propulsion Laboratory (JPL), California Institute of Technology, and was sponsored by NASA. The author is indebted to Dr. A. Y. Lee, the AACS Team Lead, and his other colleagues at JPL for many helpful discussions. The author is also grateful to R. T. Mitchell, the Cassini Program Manager, E. H. Maize, the Program Deputy Manager, and J. L. Webster, the Spacecraft Operation (SCO) Manager for their support, as well as to S. Augenstein, the co-op student from University of Michigan, for his assistance and cooperation.

References

[1] Lee, A., "Cassini Orbiter Functional Requirements Book: Accuracy Requirements and System Capabilities," CAS-3-170, Jet Propulsion Laboratory, Internal Document, JPL D-699-205, rev. D, California Institute of Technology, Pasadena, CA, Nov. 1997

[2] Augenstein, S., and Sarani, S., "Flight Rule Regarding Parameter Adjustment of Excessive Thruster Commanding Monitor during Titan Flybys," JPL IOM SCO-03-023, July 24, 2003

[3] "Cassini Guidance Analysis Book," PD 699-409, JPL D-7841, September 1994

[4] "Cassini Mission Plan," Revision N, PD 699-100, JPL D-5564, May 2002

[5] Sarani, S., "Documentation of Recent Cassini Inertial Property, Main Engine Parameter, and RCS Thruster Magnitude Predictions for AACS," IOM SCO-02-039 CAS, June 12, 2002

[6] Sarani, S., "New SOI and Probe Relay Parameters for A8 Flight Software," IOM SCO-02-038 CAS, June 12, 2002

[7] Coustenis, A., and Taylor, F., "Titan, The Earth-Like Moon," World Scientific Publishing Company, ISBN 981-02-3921-1, pp. 53-61, Copyright 1999

[8] "Cassini Physical Constants Document," Jet Propulsion Laboratory, Internal Document, Revision 1, 699-117, JPL D-10759, May 15, 1993

[9] Adler, M., "Titan Atmosphere Model," JPL IOM 312/95.5-4351, March 17, 1995

[10] Price, H.,"Cassini Projected Area Plots, No. 2," JPL IOM 3522-92-216, October 16, 1992

[11] Lee, A.,"First Titan flyby – Three AACS Issues," JPL IOM SCO-00-041, September 15, 2000

[12] "Cassini Spacecraft Flight Rules and Constraints," PD 699-270, JPL D-11202, FR07B131, June 13, 2003

[13] Lee, A., "Model-Based Thruster Leakage Monitor for the Cassini Spacecraft," Journal of Spacecraft and Rockets, Vol. 36, No. 5, September-October 1999

[14] Yelle, R. V., Strobell, D. F., Lellouch, E., and Gautier, D. "Engineering Models for Titan's Atmosphere,"A report to Huygen's science working team, 1994

[15] Vervack, Jr., R. J., Sandel, B. R., Strobell, D. F., "First Results From a Reanalysis of the Voyager 1 Ultraviolet Spectrometer Solar Occultations by Titan," Icarus, September 1999

[16] Wong, E., "Cassini Control Analysis Book," JPL D-9638, PD 699-410, November 12, 1998

[17] "Cassini Orbiter Functional Requirements Book, Inertial Properties Requirements," CAS-3-200, Rev. B, July 30, 1997